Supporting Information

Solution-processed Ni-based nanocomposite electrocatalysts: An approach to highly efficient Electrochemical Water Splitting

Jaume Noguera-Gómez, [†1] Miguel García-Tecedor, [†2‡] Juan Francisco Sánchez-Royo, [1] Luisa María Valencia Liñán, [3] María de la Mata, [3] Miriam Herrera-Collado, [3] Sergio. I. Molina,[3] Rafael Abargues,[1*] Sixto Gimenez[2*]

[1] UMDO, Instituto de Ciencia de los Materiales, Universidad de Valencia, P.O. Box 22085, 46071 Valencia, Spain

[2] Institute of Advanced Materials (INAM), Universitat Jaume I, Avenida de Vicent Sos Baynat, s/n, 12006 Castelló de la Plana, Spain

[3] Departamento de Ciencia de los Materiales e I. M. y Q. I Facultad de Ciencias, Universidad de Cádiz Campus Río San Pedro, s/n, 11510 Puerto Real, Cádiz, Spain

[‡] Present Address: Photoactivated Processes Unit, IMDEA Energy Institute, Parque Tecnológico de Móstoles, Avda. Ramón de la Sagra 3, 28935 Móstoles, Madrid, Spain.

[†] These authors contributed equally to this work.

Corresponding author: Rafael.Abargues@uv.es, sjulia@uji.es

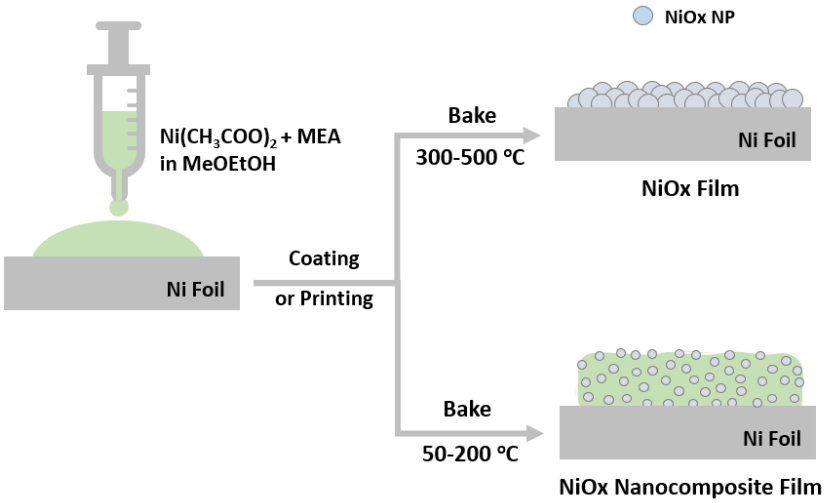

Figure S1. Schematic illustration of the solution-processed synthesis of the NiO_x catalytic electrodes.

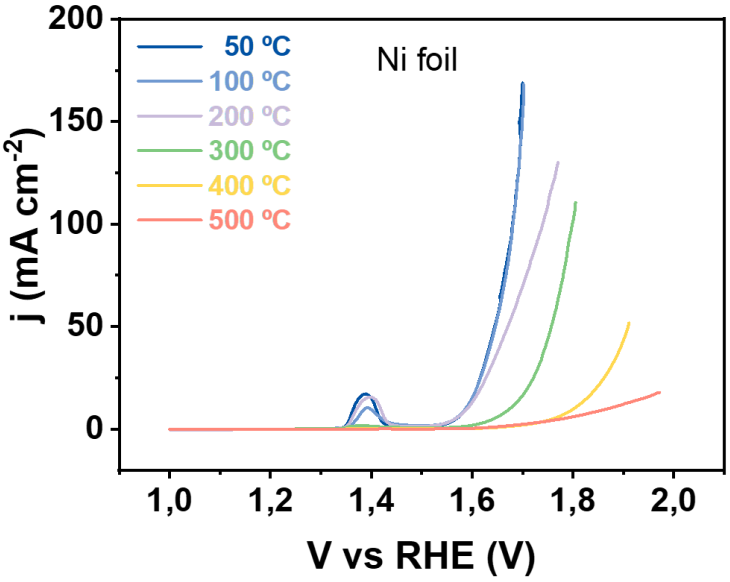

Figure S2. Linear Sweep Voltammetry of the NiO_x samples baked at different temperatures in 1M KOH electrolyte (pH = 13.6).

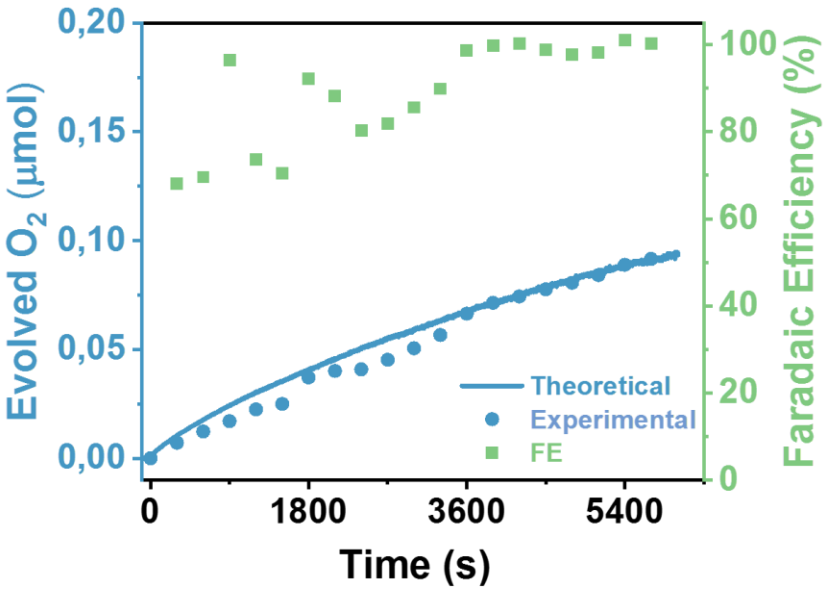

Figure S3. Oxygen evolution and faradaic efficiency (FE) on the optimal NiO_x catalyst (baked at 50 ºC) at 1.7 V vs. RHE.

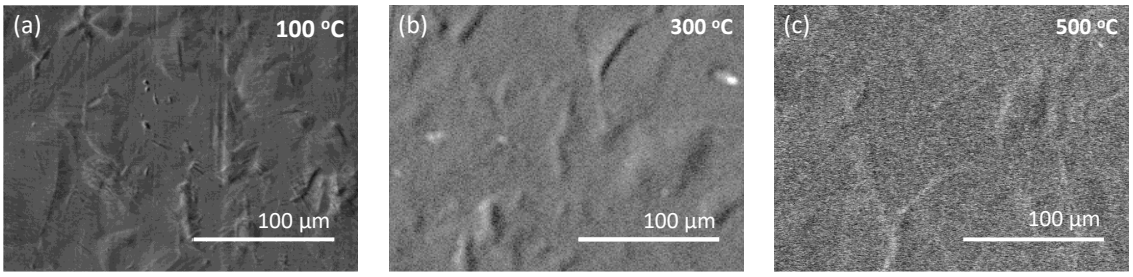

Figure S4. SEM images of NiO_x thin films baked at different temperatures. (a) 100 ºC, (b) 300 ºC, and (c) 500 ºC.

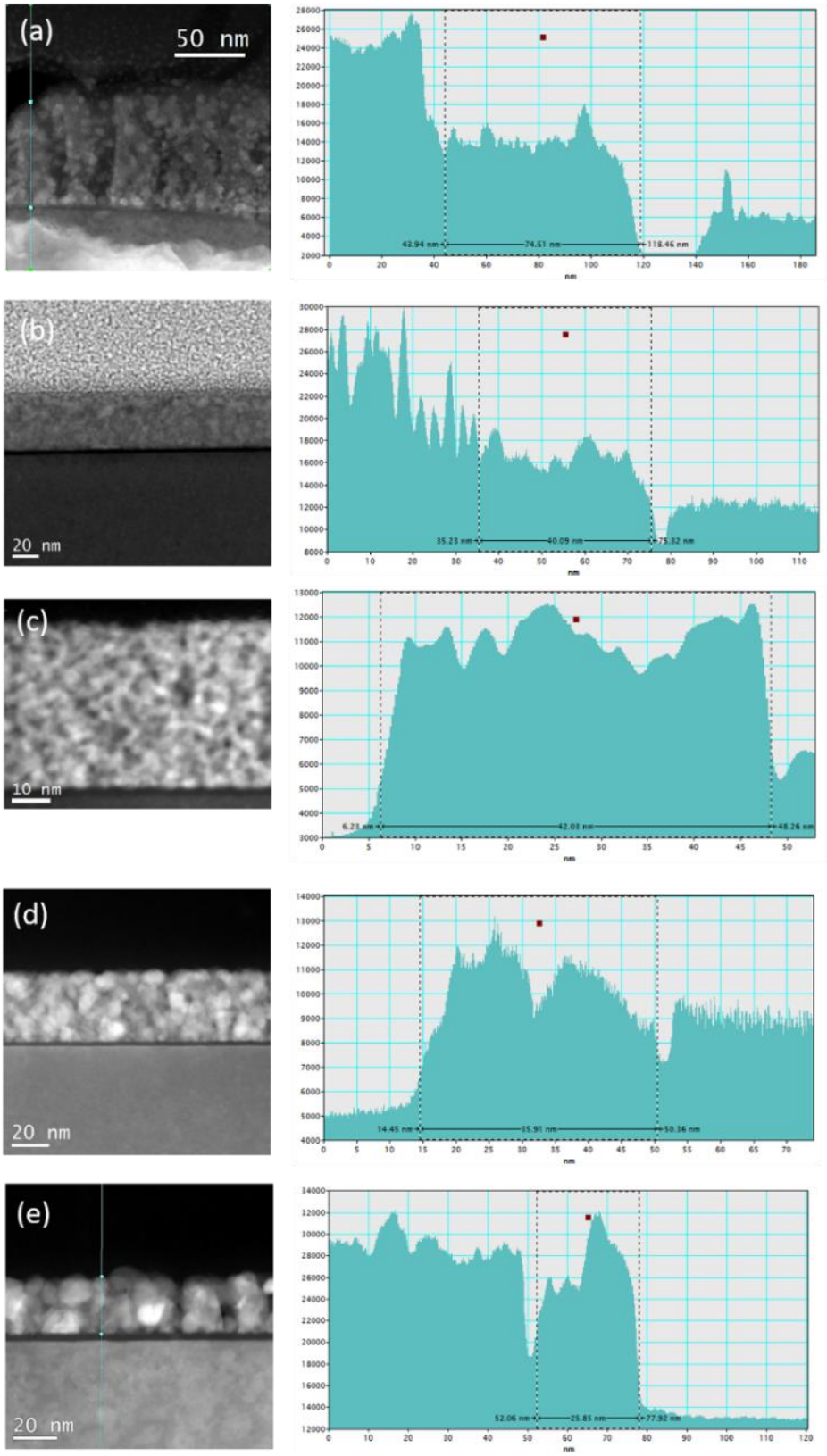

Figure S5. HAADF-STEM images and intensity profiles for the determination of NiO_x film thickness for the different baking temperatures. (a) 100 ºC, (b) 200 ºC, (c) 300 ºC, (d) 400 ºC, (e) 500 ºC.

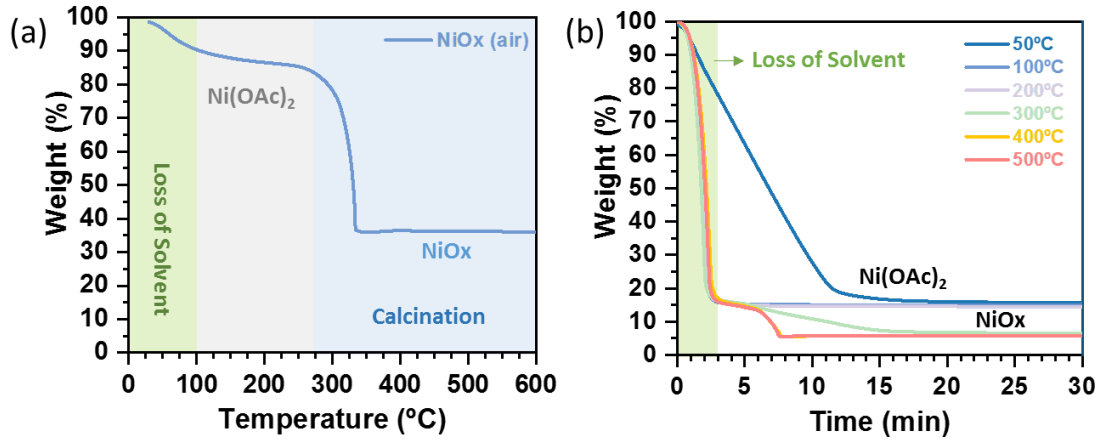

Figure S6. TGA. (a) Weight % vs. temperature. (b) Isothermal weight % vs. time for temperatures between 50 and 500 ºC.

Figure S6a shows the thermogravimetric analysis (TGA) of a dried powder prepared from a precursor solution of NiO_x (0.45 M $Ni(OAc)_2$, 0.45 M MEA in 2-methoxyethanol). From 30 to 100 °C, TGA shows a mass loss of 11 wt. % due to the evaporation of residues of solvents (2-methoxyethanol and water) and some MEA. From 100 to 275 °C, the mass loss is about 6.1 wt. % because of the complete evaporation or decomposition of MEA. A significant mass loss of 40.3 wt. % takes place from 250 to 400 °C. This is ascribed to the desorption and decomposition of acetate groups[1] from Ni-based clusters during the formation of NiO_x. Similar behavior has been reported in the synthesis of ZnO films.[2] From 320 to 600 °C, a mass loss of only 2.1% is observed due to the combustion of organic residues. The final solid content is 35.8 wt. % and can be ascribed to the formation of NiO. This result is in good agreement with the hypothetical full calcination of $Ni(OAc)_2$ to NiO (34,5 wt. %).

Figure S6b shows an isothermal weight loss of the precursor NiO_x vs. time solution for different temperatures between 50 and 500 ºC. Within the first 3 min, a weight loss of 85 wt. % takes place due to the evaporation of 2-methoxyethanol and water, except for 50 ºC that takes 12 minutes. From 50 to 200 ºC, the weight loss levels off to show a final solid content around 16 wt.%. From 300 to 500ºC, a weight loss of 10 wt. % takes place after 15 min. A solid content around 5.7 wt. % is measured once acetate and other organic species are removed. These results suggest that the reaction generally takes place at any temperature within the first 20 min, and consequently, longer baking times are not needed. If we compare the solid content of samples baked at low temperatures (50, 100, and 200 ºC) and high temperatures (300, 400, and 500 ºC), we observe a constant wt. ratio of 2.7, which is in good agreement with 2.9 wt. ratio of $Ni(OAc)_2$/NiO. TGA isotherms can therefore confirm the presence of $Ni(OAc)_2$ at low baking temperatures.

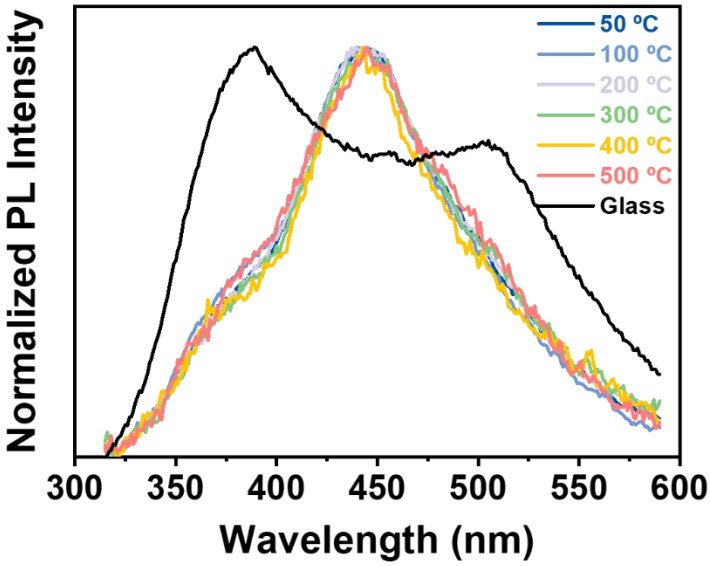

Figure S7. Normalized photoluminescence emission of the NiO_x samples baked at the different temperatures and the glass substrate as reference. The PL response of the glass substrate features a broad emission between 300 and 600 nm with two prominent peaks located at 390 and 508 nm.

S8: XPS analysis

A complete analysis of the surface properties of NiOx films by XPS is described here. **Figure 4** (a) and (b) (main text) show the XPS spectra at the energy region of the O 1s and Ni 2p core levels measured in the samples baked from 100 to 500 ºC. Below 200 ºC, both core levels seem to be quite well reproduced by a single component; the O 1s by a singlet peak centered at 532.0 eV and the Ni 2p by a spin-orbit doublet whose j=3/2 broad component lies at 856.5 eV with a spin-orbit splitting of 17.7 eV. The Ni 2p main doublet is accompanied by its typical shake-up satellite located at ~6 eV from the main doublet to higher binding energies. The presence of these core levels is characteristic of Ni(II) species, which we attribute to $Ni(OH)_2$.[3-4]

From 200 ºC, both the O 1s and Ni 2p spectra are red-shifted. We observe the new O 1s and Ni 2p core-level components located at lower binding energies. In particular, the O 1s spectrum of the sample baked at 200 ºC is composed of a broad and intense peak centered at ~531.5 eV and a second new peak located at ~529.5 eV. As the bake temperature increases, the low binding-energy O 1s peak becomes more intense, at the expense of the broad peak located at 531.5 eV. Deconvolution of the O 1s spectra (**Figure 4**a) shows three singlets located at 532.1 ± 0.2 eV (already attributed to OH^- species), 531.4 ± 0.2 eV, and 529.7 ± 0.1 eV. These two latter O 1s singlets are ascribed to the presence of O^{-2} species. The integrated intensity of the O^{-2} component located at 531.4 eV and that for OH^- located at 532.1 eV appear to follow a 1:1 ratio for samples prepared at temperatures higher than 200 ºC, which is indicative of the presence of NiOOH.[5] The third O^{-2} singlet, located at 529.7 eV, is indicative of the presence of NiO.[4-6] This assignment of the different O 1s components allows proposing the following composition of the samples prepared at different temperatures. $Ni(OH)_2$ seems to be the main form of Ni^{+2} in samples prepared at low temperatures (100 ºC). However, preparation temperatures around 200 ºC rapidly favor the formation of Ni^{+3} species in the form of NiOOH and Ni^{+2} in the form of NiO, which becomes dominant as the preparation temperature increases.

Deconvolution of the Ni 2p spectra (**Figure 4**b) is difficult to perform. However, to assess the consistency of the behavior proposed above for the composition of the samples prepared at different temperatures, we have deconvoluted the Ni 2p spectra shown in **Figure 4**b in three different Ni 2p components, by assuming that the composition ratio

among NiO, NiOOH and $Ni(OH)_2$ is that given by the O 1s spectra (**Figure 4**a). The result of this analysis is included in **Figure 4**b, which is consistent with the presence of Ni 2p components whose j=3/2 peak are located at 855.0 eV (NiO), 855.2 (NiOOH), and 856.5 eV ($Ni(OH)_2$).[4-6]

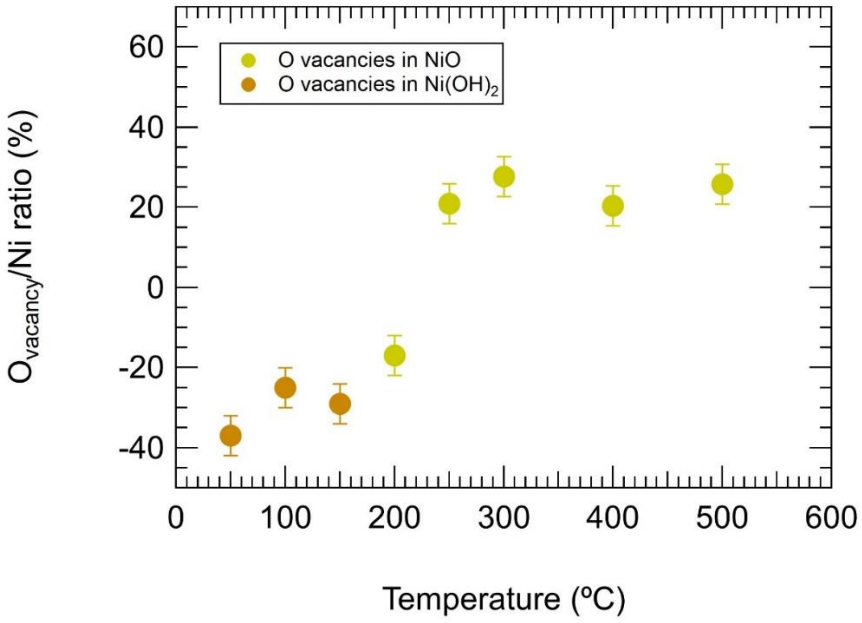

Figure S8.- Surface oxygen vacancy ratio in the NiO_x samples estimated from XPS measurements showed as Figure 4 in the main text.

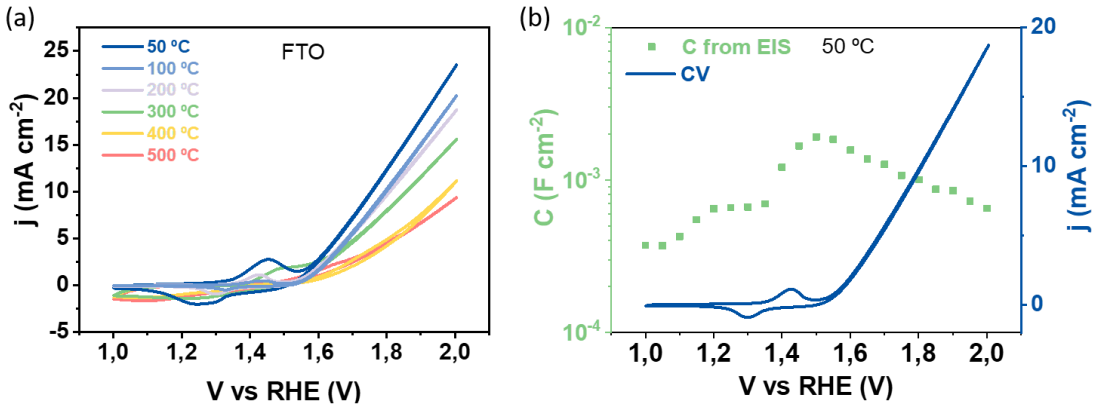

Figure S9. (a) Cyclic voltammograms of the different samples deposited on FTO substrates. (b) Extracted capacitance versus applied potential and cyclic voltammetry of the 50 ºC sample.

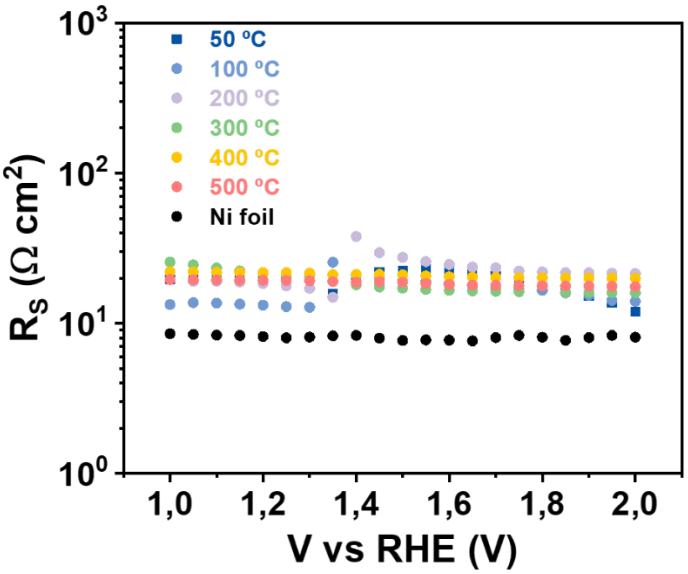

Figure S10. Series resistance (R_s) versus applied potential of FTO/NiO_x films at each baking temperature. The series resistance of a Ni/NiO_x film is also showed for comparison.

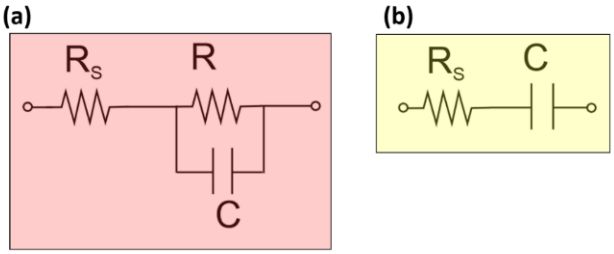

Figure S11. Equivalent circuits employed to fit the raw impedance data. R_s is series resistance, R is the film resistance (dominated by the charge transfer to the electrolyte) and C is the capacitance.

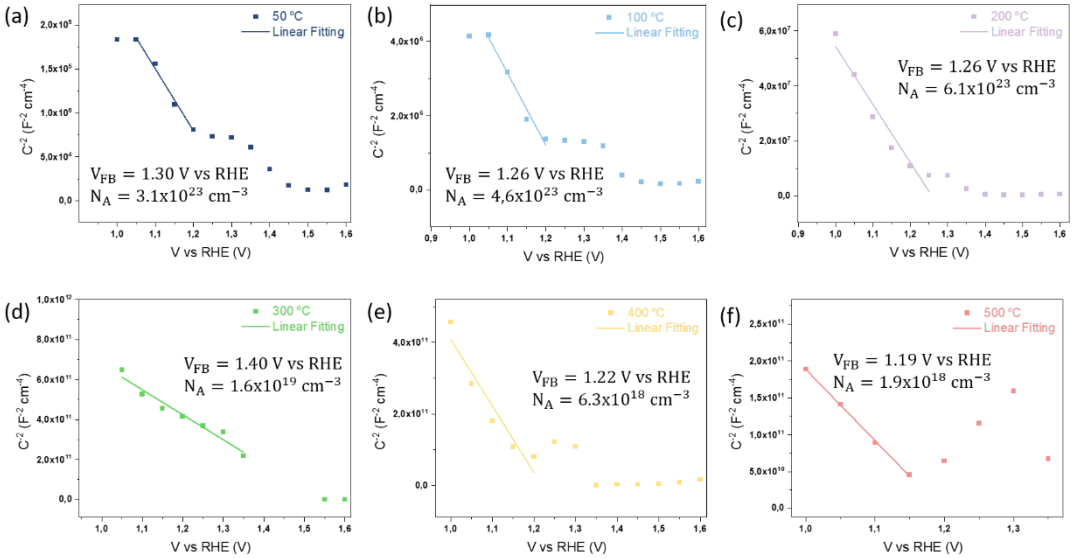

Figure S12. Mott-Schottky analysis of the FTO/NiO_x films baked at different temperatures (a) 50 ºC, (b) 100 ºC, (c) 200 ºC, (d) 300 ºC, (e) 400 ºC, (f) 500 ºC. The flatband potential (V_{FB}) and acceptor density (N_A) are indicated in each plot. The details of the impedance measurements are included in the main text (Experimental Methods).

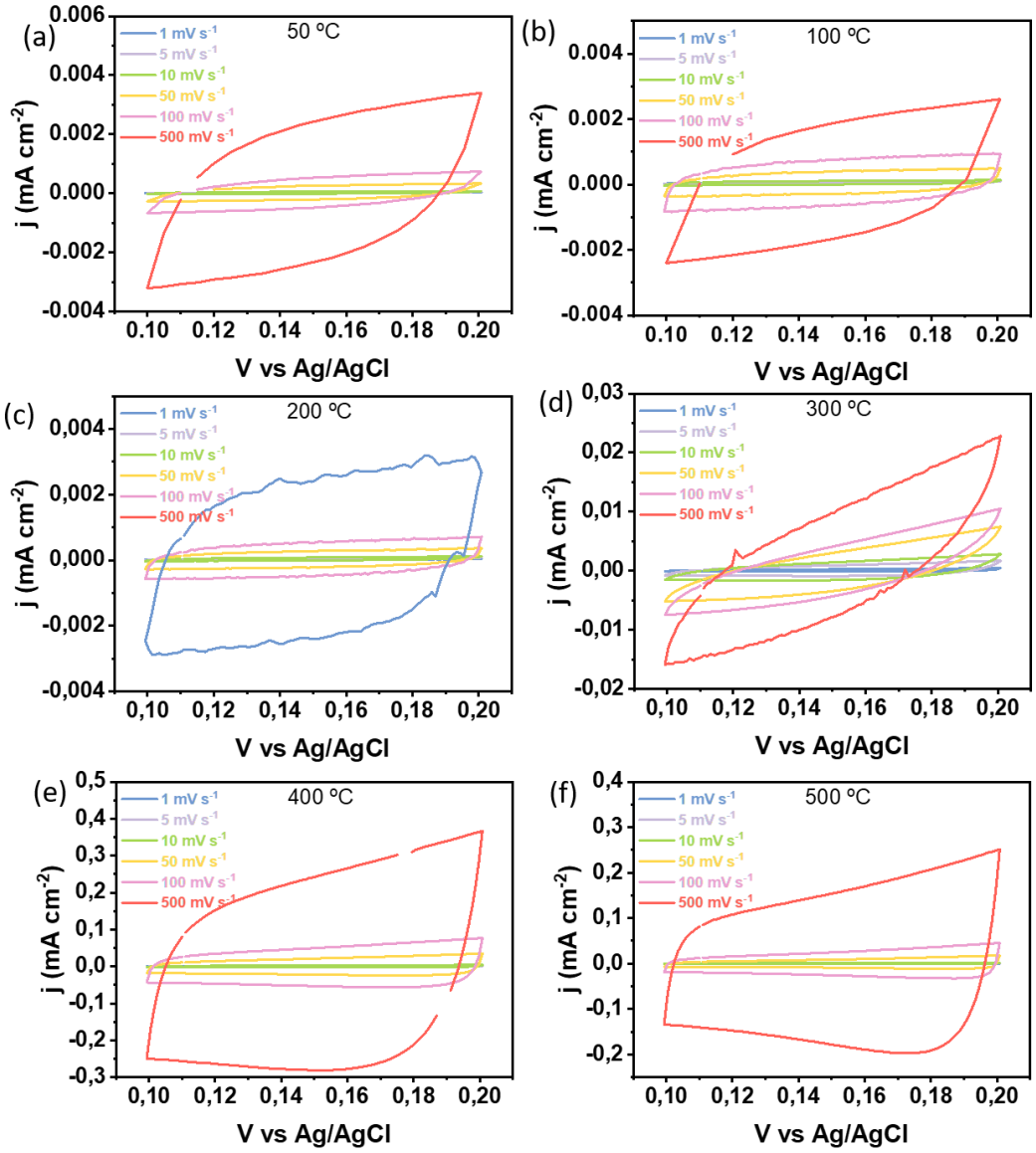

Figure S13. Cyclic voltammograms at different scan rates of the NiO_x films baked at different temperatures in 1M KOH electrolyte (pH = 13.6) to determine the electrochemical surface area (ECSA).

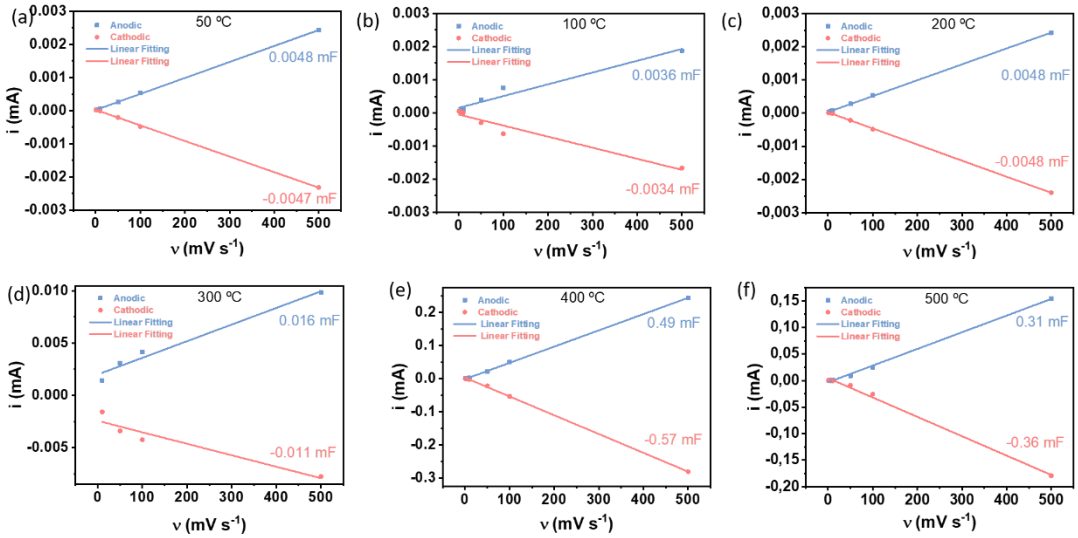

Figure S14. Electrochemical surface area (ECSA) of the NiO_x samples baked at different temperatures in 1M KOH electrolyte (pH = 13.6).

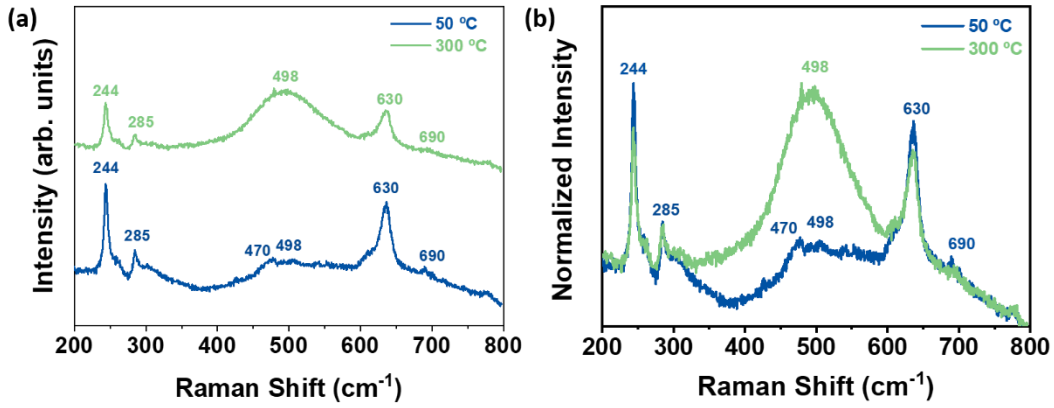

Figure S15. (a) Stacked and (b) normalized Raman spectra of the NiO_x films baked at 50 ºC and 300 ºC after electrochemistry.

Table S1. Benchmarking of the most active undoped NiO_x based electrocatalysts for water oxidation reported.

Material	Support	η at 10 mA cm^{-2} (mV)	Tafel slope (mV dec^{-1})	pH	Reference
NiO_x	SiO_2	450 (at 1 mA cm^{-2})	72	14	[7]
NiO	TiO_2	320	52	14	[8]
Ni/NiO	Graphene Oxide	270	46	13.4	[9]
NiO	Au	280 (at 1 mA cm^{-2})	40	13.4	[10]
Ni/NiO	Carbon Fiber	300	60	14	[11]
NiO_x	MWCNTs	200	60	9.2	[12]
NiO	Ni foam	310	54	14	[13]
NiO	Glassy C	240	73	14	[14]
NiO_x	Ni foil	358	73	13.6	This work

Table S2. Solid fraction (wt %) for different baking temperatures after 30 min taken from Figure S6b

Temperature ºC	Solid fraction Wt. % @ 30 min
50	15.8
100	14.9
200	14.5
300	6.7
400	5.9
500	5.7

Table S3. Electrochemical Surface Area (ECSA) determined from Figure S13 and S14 for the NiO_x samples baked at different temperatures in 1M KOH electrolyte (pH = 13.6).

Bake temperature (°C)	**Capacitance (μF)**	**ECSA (cm^2)**
50	0.48	0.12
100	0.35	0.09
200	0.48	0.12
300	13	0.34
400	540	1.32
500	330	8.37

References

(1) Ong, B. S.; Li, C.; Li, Y.; Wu, Y.; Loutfy, R. Stable, Solution-Processed, High-Mobility ZnO Thin-Film Transistors. *Journal of the American Chemical Society* **2007,** *129* (10), 2750-2751, DOI: 10.1021/ja068876e.
(2) Hosono, E.; Fujihara, S.; Kimura, T.; Imai, H. Non-Basic Solution Routes to Prepare ZnO Nanoparticles. *Journal of Sol-Gel Science and Technology* **2004,** *29* (2), 71-79, DOI: 10.1023/B:JSST.0000023008.14883.1e.
(3) Liang, Y.; Sherwood, P. M. A.; Paul, D. K. Valence and core photoemission of the films formed electrochemically on nickel in sulfuric acid. *Journal of the Chemical Society, Faraday Transactions* **1994,** *90* (9), 1271-1278, DOI: 10.1039/FT9949001271.
(4) Grosvenor, A. P.; Biesinger, M. C.; Smart, R. S. C.; McIntyre, N. S. New interpretations of XPS spectra of nickel metal and oxides. *Surface Science* **2006,** *600* (9), 1771-1779, DOI: https://doi.org/10.1016/j.susc.2006.01.041.
(5) Payne, B. P.; Biesinger, M. C.; McIntyre, N. S. The study of polycrystalline nickel metal oxidation by water vapour. *Journal of Electron Spectroscopy and Related Phenomena* **2009,** *175* (1), 55-65, DOI: https://doi.org/10.1016/j.elspec.2009.07.006.
(6) Weidler, N.; Schuch, J.; Knaus, F.; Stenner, P.; Hoch, S.; Maljusch, A.; Schäfer, R.; Kaiser, B.; Jaegermann, W. X-ray Photoelectron Spectroscopic Investigation of Plasma-Enhanced Chemical Vapor Deposited NiOx, NiOx(OH)y, and CoNiOx(OH)y: Influence of the Chemical Composition on the Catalytic Activity for the Oxygen Evolution Reaction. *The Journal of Physical Chemistry C* **2017,** *121* (12), 6455-6463, DOI: 10.1021/acs.jpcc.6b12652.
(7) Wu, L.-K.; Hu, J.-M.; Zhang, J.-Q.; Cao, C.-N. A silica co-electrodeposition route to highly active Ni-based film electrodes. *Journal of Materials Chemistry A* **2013,** *1* (41), 12885-12892, DOI: 10.1039/C3TA12503C.
(8) Zhao, Y.; Jia, X.; Chen, G.; Shang, L.; Waterhouse, G. I. N.; Wu, L.-Z.; Tung, C.-H.; O'Hare, D.; Zhang, T. Ultrafine NiO Nanosheets Stabilized by TiO2 from Monolayer NiTi-LDH Precursors: An Active Water Oxidation Electrocatalyst. *Journal of the American Chemical Society* **2016,** *138* (20), 6517-6524, DOI: 10.1021/jacs.6b01606.
(9) Munir, A.; Haq, T. u.; Qurashi, A.; Rehman, H. u.; Ul-Hamid, A.; Hussain, I. Ultrasmall Ni/NiO Nanoclusters on Thiol-Functionalized and -Exfoliated Graphene Oxide Nanosheets for Durable Oxygen Evolution Reaction. *ACS Applied Energy Materials* **2019,** *2* (1), 363-371, DOI: 10.1021/acsaem.8b01375.
(10) Fominykh, K.; Feckl, J. M.; Sicklinger, J.; Döblinger, M.; Böcklein, S.; Ziegler, J.; Peter, L.; Rathousky, J.; Scheidt, E. W.; Bein, T. Ultrasmall dispersible crystalline nickel oxide nanoparticles as high-performance catalysts for electrochemical water splitting. *Advanced Functional Materials* **2014,** *24* (21), 3123-3129.
(11) Zhang, Z.; Liu, S.; Xiao, F.; Wang, S. Facile synthesis of heterostructured nickel/nickel oxide wrapped carbon fiber: flexible bifunctional gas-evolving electrode for highly efficient overall water splitting. *ACS Sustainable Chemistry & Engineering* **2017,** *5* (1), 529-536.
(12) Yu, X.; Xu, P.; Hua, T.; Han, A.; Liu, X.; Wu, H.; Du, P. Multi-walled carbon nanotubes supported porous nickel oxide as noble metal-free electrocatalysts for efficient water oxidation. *International journal of hydrogen energy* **2014,** *39* (20), 10467-10475.
(13) Babar, P.; Lokhande, A.; Gang, M.; Pawar, B.; Pawar, S.; Kim, J. H. Thermally oxidized porous NiO as an efficient oxygen evolution reaction (OER) electrocatalyst for electrochemical water splitting application. *Journal of industrial and engineering chemistry* **2018,** *60*, 493-497.

(14) Tahir, M.; Pan, L.; Zhang, R.; Wang, Y.-C.; Shen, G.; Aslam, I.; Qadeer, M.; Mahmood, N.; Xu, W.; Wang, L. High-valence-state NiO/Co3O4 nanoparticles on nitrogen-doped carbon for oxygen evolution at low overpotential. *ACS Energy Letters* **2017,** *2* (9), 2177-2182.